https://doi.org/10.5194/egusphere-2022-1178
Preprint. Discussion started: 2 November 2022

Time-dependent Frictional Properties of Granular Materials Used In Analogue Modelling: Implications for mimicking fault healing during reactivation and inversion

Michael Rudolf[1,2], Matthias Rosenau[2], and Onno Oncken[2]

[1]Institute of Applied Geosciences, Fachgebiet Ingenieurgeologie, Technical University Darmstadt, Schnittspahnstraße 9, 64287 Darmstadt, Germany
[2]Lithosphere Dynamics, Helmholtz Centre Potsdam, GFZ German Research Centre for Geosciences, Telegrafenberg, 14473 Potsdam, Germany

Correspondence: Michael Rudolf (rudolf@geo.tu-darmstadt.de)

Abstract. Analogue models are commonly used to model long-term geological processes such as mountain building or basin inversion. The majority of these models use granular materials like sand or glass beads to simulate the brittle behaviour of the crust. In granular materials deformation is localized into shear bands that act as analogues to natural fault zones and detachments. Shear bands aka faults are persistent anomalies in the granular package and are frequently reactivated during an experimental run. This is due to their lower strength in comparison to the undeformed bulk material. When fault motion stops, time dependent healing immediately starts to increase the strength of the fault. Therefore, older faults show a higher strength in comparison to younger faults. This time dependent healing, also called time consolidation, can therefore affect the structural style of an analogue model due to evolution of fault strength over time. Time consolidation is a well known mechanism in granular mechanics but remains poorly characterized for analogue materials and on the timescales of typical analogue models. In this study, we estimate the healing rate of several analogue materials and evaluate the consequences on the reactivation potential of analogue faults. We find that the healing rates are generally below 3% per tenfold increase in hold time which is comparable to natural fault zones. We qualitatively compare the frictional properties of the materials with grain characteristics and find a weak correlation of healing rates with sphericity and friction with an average quality score. In models where predefined faults exist or reactivation is forced by blocks, the stability region of fault angles that can be reactivated can accordingly decrease by up to 7° over the duration of 12 hours. The stress required to reactivate a preexisting fault can double in the same time which may favor the creation of new faults. In a basin inversion scenario, normal faults can not be inverted due to severe misorientation and therefore time consolidation plays only a minor additional role for such models.

https://doi.org/10.5194/egusphere-2022-1178
Preprint. Discussion started: 2 November 2022

1 Introduction

Crustal tectonics involves fault localization and reactivation as well as changes in fault slip rates (transients) and slip directions (inversion) over timescales from hundreds of years (seismic cycle) to tens of millions of years (Wilson cycle). For example, the inversion of sedimentary basins is governed by a change from extensional to compressional tectonics which leads to the shortening of basin structures (Turner and Williams, 2004). In such a scenario, shortening can be accommodated by either the reactivation of pre-existing structures or the formation of new faults. Structural inhomogeneities that localize deformation during inversion are mainly the normal faults formed under extension and stratigraphic layers of the basin sediments. In many cases, newly formed structures link with existing ones which forms shortcuts to create the energetically most favourable fault configuration. This interplay of extensional and compressional tectonics as well as inherited and newly formed structures creates a complex structural inventory that is inherent to many sedimentary basins world-wide which are regions that are of high societal and economic importance hosting e.g. earthquakes, ore deposits and hydrocarbon resources (Buchanan et al., 1995; Turner and Williams, 2004).

Many experimental studies show that the localization of brittle deformation into narrow bands is governed by the strain weakening characteristics of rocks. As a result, faults are mechanically weaker than the undeformed host rock and thus are reactivated when subjected to stress (Sibson, 1980). However, other factors influence the reactivation characteristics of a fault, most notably the orientation of stresses with respect to the fault. Additionally, fluid pressure, the exact mechanical properties of the fault zone and interaction with other faults can prevent or promote fault reactivation (Niemeijer et al., 2008). There is a multitude of numerical, mechanical and analogue modelling studies that address the influence of these parameters on fault reactivation (e.g. Jara et al., 2018; Yagupsky et al., 2008; Panien et al., 2006, and references in Table 2). Especially in analogue models, the reactivation of normal faults is largely dependent on the orientation as the other factors are rarely incorporated into the model (Bonini et al., 2012).

Analogue modelling is a technique that is widely used for tectonic modelling in general and basin inversion models in particular because it is inherently 3D and can handle discontinuities with large displacements which is challenging for most numerical approaches. It is built around the principle of similitude (Hubbert, 1937) which states that a system can be modeled by a geometrically smaller model if the governing dimensionless properties are the same. This is frequently used for geological modelling of complex tectonic processes and in other disciplines where numerical approaches are still not entirely feasible, such as hydraulic engineering. While numerical models are easy to quantify and there is a large freedom in defining material properties, analogue modellers have access to only a small range of suitable materials for specific problems. In the past this has been limited to various natural (e.g. sands) and artificial granular materials (e.g. glass beads) as frictional components (Klinkmüller et al., 2016; Ritter et al., 2016a, 2018), sometimes mixed with more fine-grained (powder) materials, like flour and plaster, to increase the cohesion according to scaling laws (Poppe et al., 2021a). Models involving viscous layers (e.g. lower crust, salt) typically use silicone oils (PDMS) (Rudolf et al., 2016) and other visco-elastic materials. Recently, there is a surge in new materials to fine-tune specific properties of the brittle or ductile layer. However, all analogue models rely on

https://doi.org/10.5194/egusphere-2022-1178
Preprint. Discussion started: 2 November 2022

accurate and suitable material characterisation to be able to quantify the similarity of stresses and ultimately the similitude of the model.

A property that has received little to no attention is the time dependency of frictional material properties, in particular healing (i.e. static strengthening). In this context we identify two major implications for the analysis of reactivated structures with analogue models. The first is that due to the consolidation of granular materials over time, the reactivation strength increases which could lead to problems with repeatability when there are differences in the timing of extensional and compressional phases between model runs. In the engineering community this effect is known as time consolidation and usually is considered as being minor in typical analogue materials (Schulze, 2008). However, most studies on time consolidation focus on large piles or silos with several meters overburden material and not a few centimeters as in analogue models. Due to the increase of shear resistance over time, reactivation angles and structures could differ between a model that has for example a one minute static phase between extension and compression in comparison to a model that has a several hours stop between extension and compression. Models with erosion and sedimentation are especially prone to this effect because they usually require the model to be stopped for some time to add or remove material. Secondly, natural faults also show time dependent healing due to pressure solution, Ostwald ripening and fracture sealing by hydrothermal minerals (Karner et al., 1997; Niemeijer et al., 2008). At short time scales of the seismic cycle, this behaviour is described by the dimensionless healing rate b in the rate-and-state framework (Dieterich, 2007) while for longer tectonic time scales the quantification is more challenging (Yasuhara et al., 2005). To accurately mimic this natural healing in analogue models it is required that the analogue materials show quantitatively similar characteristics as rocks, e.g. the same healing rate b.

Consequently, the aim of this study is: (1) to quantify the healing properties of analogue materials from different laboratories and to relate them to first order observable grain characteristics, (2) to analyze the impact on the reactivation angles during typical analogue models of basin inversion, and (3) to examine the possible use of certain materials as analogues for naturally healing faults. To build a database of materials we reached out to 14 laboratories to send us samples of their current materials and compared them to materials from the archive at the Helmholtz Laboratory for Tectonic Modelling (Table 1). The material properties were characterized by standardized ring-shear tests and slide-hold-slide tests. Furthermore, we used image analysis to gather more detailed information on grain size distributions, grain shapes and grain surface features for each material. The results are then used to review typical analogue modelling schemes and to probe possible scenarios under which the materials may or may not be suitable for modelling.

2 Methodology

2.1 Ring-shear Tester Setup

We use a RST-01.pc (Schulze, 1994) ring-shear tester to measure the frictional properties of the dry granular materials. The method is well established for analog materials (Lohrmann et al., 2003; Panien et al., 2006; Klinkmüller et al., 2016; Montanari et al., 2017) and follows international standards for powder and bulk material testing (ASTM, 2016). The machine consists of a rotating, ring-shaped shear cell onto which normal stress is applied using a stationary lid. The shear stress required to hold

https://doi.org/10.5194/egusphere-2022-1178
Preprint. Discussion started: 2 November 2022

the lid in place is measured using two tie rods that are each attached in series to force transducers. To improve the contact of the cell and lid with the material, the surface of the lid, as well as the bottom of the shear cell is structured with slats and grooves. Normal stress is applied through a cantilever system with a moving mass and therefore is instantly adjusted by gravity, in contrast to other mechanical tests where the stresses are adjusted with a servo-hydraulic or electronic system. During each measurement, the shear velocity, shear stress, normal stress and lid position is monitored. Further information on the setup and device is available in Schulze (1994), Lohrmann et al. (2003) and Ritter et al. (2016a).

The testing procedure follows standardized procedures for sample preparation (Lohrmann et al., 2003; Klinkmüller et al., 2016), testing procedure (Lohrmann et al., 2003; Ritter et al., 2016a) and data analysis (Rosenau et al., 2018a; Rudolf et al., 2021). All samples are first oven dried to remove excess humidity and then stored in the air-conditioned laboratory for several days to equilibrate with ambient laboratory conditions of $T = 25°C$ and ≈ 50 % humidity. The samples are sieved using the SM sieve into the cell from a height of ca. 30 cm and above, ensuring a similar package density for each test (Lohrmann et al., 2003). We do not use the same sieve as Klinkmüller et al. (2016), called 'GeoMod'-sieve because for our measurements the samples are pre-sheared and the package density after sieving is not a primary concern. Excess material is scraped off and the weight of the material is determined. After inserting the cell into the tester, the normal stress is applied and the shear procedure is started. Each property has a specific shear procedure which is outlined in the respective subsections (Section 2.2 for friction μ and cohesion C, Section 2.3 for the healing rate b).

2.2 Mohr-Coulomb Friction

Most tectonic analogue models use dry granular materials as analogues for crustal rocks in the brittle regime (Klinkmüller et al., 2016) with only a few exceptions that use wet clay or other non granular material (Bonini et al., 2012). The greatest advantage of granular materials is that they obey the empirical Mohr-Coulomb criterion (Equation 1):

$$\tau = \mu\sigma + C \tag{1}$$

Granular analogue materials show friction coefficients μ and cohesions C that are comparable (in case of C when scaled) to typical crustal rocks: In particular sands with $\mu = 0.6$ to 0.7 and C in the order of tens of Pa (scaling to few MPa) or glass beads with $\mu = 0.4$ to 0.5 and C in the order of few Pa. Moreover, the granular materials show stress-strain relationships similar to crustal rocks involving strain weakening and static healing (Lohrmann et al., 2003; Ritter et al., 2016a). This gives rise to three different coefficients of friction μ and cohesion C attributed to different stages of fault evolution (Lohrmann et al., 2003): The highest strength μ_{peak} is reached during initial shearing of undisturbed granular materials and therefore is analogous to the strength of undeformed rock (static friction). With continued shearing the materials looses strength (strain weakening) and reaches a lower strength during stable sliding μ_{stable} corresponding to the sliding resistance of a fault zone (sliding, dynamic or kinetic friction). If a material has been sheared the granular fault zone is persistent and leaves a heterogeneity with lower density in the bulk material. If resheared, a new peak strength $\mu_{reactivation}$ occurs which reflects the strength of a preexisting fault zone and which usually is higher than the stable sliding strength but lower than the initial peak strength. Consequently,

https://doi.org/10.5194/egusphere-2022-1178
Preprint. Discussion started: 2 November 2022

Table 1. Materials and references where the data can be found.

Material	Reference
Quartz sands	Klinkmüller et al. (2016); Ritter et al. (2016b); Rosenau et al. (2018a, b); Zwaan et al. (2018); Willingshofer et al. (2018); Román-Berdiel et al. (2019); Warsitzka et al. (2019b); Schmid et al. (2020); Poppe et al. (2021b)
Corundum sands	Klinkmüller et al. (2016); Schmid et al. (2020)
Feldspar sands	Klinkmüller et al. (2016); Willingshofer et al. (2018); Zwaan et al. (2018)
Garnet sands	Klinkmüller et al. (2016)
Glass beads	Klinkmüller et al. (2016); Warsitzka et al. (2019b); Pohlenz et al. (2020a, b, c)
Zircon sands	Klinkmüller et al. (2016)
Foam glass	Warsitzka et al. (2019a)

models with granular materials localize deformation into narrow shear bands because of their lower sliding resistance and reactivate these structures under favourable circumstances due to the lower reactivation strength. From now on we will refer to these three friction coefficients by their shortened versions μ_p, μ_s and μ_r throughout this study. Note that corresponding cohesions C_p, C_s and C_r exist.

For this study we use previously published ring-shear test data by multiple sources (Table 1) which is re-picked and analyzed with the software RST-Evaluation (Rudolf and Warsitzka, 2021).

2.3 Time Consolidation (healing) and Rate-and-State Friction

In addition to the dependence on effective normal stress σ, sliding and reactivation friction coefficients μ_s and μ_r show a measurable dependence on slip rate $\dot{\delta}$ and hold time t_h, respectively. This is highly non-linear and described using the rate-and-state framework (Dieterich, 1978). This formulation is widely accepted as a good heuristic approximation of laboratory shear tests and natural phenomena (Marone, 1998; Scholz, 2002; Dieterich, 2007) where a time and strain rate dependence is observed. In general, there are two additional contributions to shear resistance: the rate effect $a ln \frac{\dot{\delta}}{\dot{\delta}^*}$ and the state effect $b ln \frac{\theta}{\theta^*}$. Both are defined by a ratio with respect to reference constants (denoted by asterisks) and added to the reference friction μ_0:

$$\tau = \sigma \left[\mu_0 + a ln \frac{\dot{\delta}}{\dot{\delta}^*} + b ln \frac{\theta}{\theta^*} \right] \tag{2}$$

https://doi.org/10.5194/egusphere-2022-1178
Preprint. Discussion started: 2 November 2022

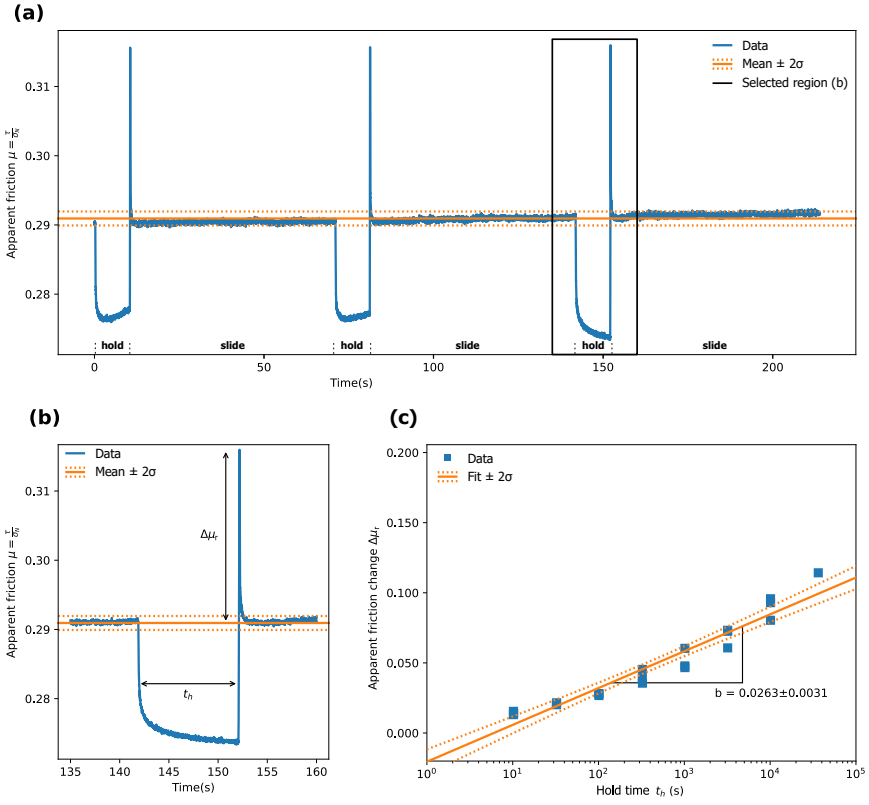

Figure 1. Time-series of one slide-hold-slide sequence and picked values. (a) Slide-hold-slide sequence of GFZ 70-110μm glass beads for $t_h = 10s$. Slide and hold phases are marked along the time axis. (b) Detailed time-series showing a single hold phase and the picked value for $\Delta\mu_r$. (c) Fit of all picked reloading friction values versus hold time. The error ranges are the 95% confidence bands for the fit.

The direct effect a, healing rate b and μ_0 are derived empirically from experimental measurements. The evolution of state θ can take several forms as a function of time (aging law, Dieterich, 1978), slip (slip law, Ruina, 1983), time dependent healing (Kato law, Kato and Tullis, 2001) or stressing rate (Nagata law, Nagata et al., 2012) which has to be assessed from experiments.

The change of strength over time in granular materials is known as time consolidation and can be very large depending on the material (Schulze, 2008). For this study we assume purely time dependent healing (aging law) and use the healing rate b to calculate the time-consolidation for each sample. We use slide-hold-slide tests to measure the healing rate following the procedure outlined in Rudolf et al. (2021, and references therein). After sample preparation (Section 2.1) and loading with $\sigma_N = 1kPa$ the sample is sheared by 10 mm at $v_L = 0.5\frac{mm}{s}$ leading to a fully developed shear zone. Then the sample is subjected to several slide-hold-slide intervals (Figure 1a). The hold intervals are increased exponentially from $t_h = 10^1$ to $10^4 s$ at increments of half a tenfold increase in time and repeated three times per interval. An additional, single hold interval of $t_h = 36000s = 10h \approx 10^{4.55}s$ gives a long term data point to each series. The full test duration is approximately 23 hours.

https://doi.org/10.5194/egusphere-2022-1178
Preprint. Discussion started: 2 November 2022

We pick the shear stress needed to reactivate the shear zone after each hold time t_h and normalize it to the mean stress during stable sliding: $\Delta\mu = \mu_r - \bar{\mu_s}$ (Figure 1b). This results in an effective stress measure assuming no cohesion. The healing rate is then the change of $\Delta\mu$ in comparison to the natural logarithm of hold time t_h (Beeler et al., 1994; Bhattacharya et al., 2017) and is obtained from as the slope of $\Delta\mu$ vs. $ln\, t_h$ (Figure 1c):

$$b = \frac{\delta\Delta\mu}{\delta ln\, t_h} \tag{3}$$

We calculate the compaction rate in the same manner by using the difference in lid position between the start and end of the hold phase. The same power-law relation is found with strong compaction for short hold phases. Values for compaction rate are negative because higher compaction results in smaller sample heights. All data is automatically picked and evaluated using a dedicated Python code published open source in the software "RST-Stick-Slipy" (Rudolf, 2021).

2.4 Grain Characteristics

Ultimately the frictional response of a bulk material is the result of granular interactions and therefore depends primarily on the geometric characteristics of the grains. The shear zones forming in the ring-shear tester usually span 11 to 16 times the mean grain size (Panien et al., 2006). The grains react to stress by creating force chains that frequently change their orientation (Cates et al., 1998; Daniels and Hayman, 2008). As a result, frictional resistance between individual grains and material elasticity has major implications on the bulk behaviour. However, it is technically very challenging to measure friction between the individual grains, and therefore we assess the tendency of each material to create locked states by using a qualitative index for several key features. We categorize the materials with three different parameters: sphericity, roundness and surface roughness. Each parameter is assigned a score from 1 to 4 which expresses the materials proneness to locking with 4='low impact' and 1='high impact'. Grain size distribution was not taken into account because comparable measurements do not exist for all materials. A heterogeneous grain size distribution changes the bulk density of the material which can influence the frictional characteristics (Lohrmann et al., 2003), however the effect is minor (Mair et al., 2002). Table 2 shows an overview of the parameters, criteria and associated literature. To account for the impact of each parameter we take a weighted average that uses the estimated effect on bulk friction from the references. We assume that this tends to reflect the amount of inter-particle locking during a hold phase and therefore also is a proxy to healing rate b.

2.5 Reactivation of Faults

The reactivation of preexisting faults in nature as well as in analogue models is primarily governed by (a) fault geometry, (b) the surrounding stress field and the (c) fault's frictional properties (Bonini et al., 2012). For natural fault systems an additional mechanism is fluid overpressure e.g. in basin sediments. However, fluids and fluid pressures cannot be accurately modelled in a scaled fashion and is thus rarely implemented in tectonic analogue models. We therefore focus on the aforementioned three factors (a) to (c) to estimate the tendency to reactivate a pre-existing fault instead of forming a new fault. We do this in a typical basin inversion scenario and use a simplified Amonton wedge model to estimate the stresses needed to push a sidewall with a

https://doi.org/10.5194/egusphere-2022-1178
Preprint. Discussion started: 2 November 2022

Table 2. Categorization scheme for granular materials with a simple 'quality score'. A lower score indicates a tendency for higher internal friction and time consolidation.

Parameter	Definition	Weight	Explanation	References
Sphericity	4 = perfect 3 = high 2 = medium 1 = low	0.4	Aspherical particles lead to higher friction.	Härtl and Ooi (2011); Chen et al. (2022)
Roundness	4 = rounded 3 = subrounded 2 = subangular 1 = angular	1.6	Round particles tend to create lower bulk friction. Angular particles favour stable sliding, while spherical particles exhibit stick-slip.	Mair et al. (2002); Suh et al. (2017)
Surface roughness	4 = smooth 3 = slightly rough 2 = shelly 1 = rough/jagged	0.9	Higher roughness leads to higher inter-particle friction resulting in higher bulk friction. Higher dilation needed for rough materials.	da Cruz et al. (2005); Tapia et al. (2019)

reactivated pre-existing fault and compare it to the stress needed to form a new fault (Collettini and Sibson, 2001; Mulugeta and Sokoutis, 2003).

The first step is to calculate the optimal fault dip angle θ_a with respect to the horizontal at which the fault forms during extension to approximate the preferred fault geometry in a first phase of the basin inversin scenario (Equation 4, Figure 2a, after Collettini and Sibson (2001)). This fault angle is defined by the friction μ of the material so that higher friction leads to steeper faults in the model.

$$\theta_a = 90° - \frac{1}{2} tan^{-1} \frac{1}{\mu} \tag{4}$$

After the extensional phase the basin switches to compression and the optimal angle for a new fault θ_p with respect to the horizontal is (Figure 2b):

$$\theta_p = \frac{1}{2} tan^{-1} \frac{1}{\mu} \tag{5}$$

To calculate what is energetically more favourable, reactivation of an inherited vs. formation of a new fault, we calculate the horizontal force F_R required to move the wedge of material formed by the side wall, surface and fault angle θ (Figure 2c). This force additionally incorporates the weight $W = \rho g h$ of the material (Mulugeta and Sokoutis, 2003). For the calculations we assume a normal stress of $\sigma_N = 1000 Pa$ analogous to the slide-hold-slide tests which corresponds to a height $h = 3.5$ to $5.5 cm$ for materials with a bulk density of $\rho = 1800$ to $3000 \frac{kg}{m^3}$, respectively:

https://doi.org/10.5194/egusphere-2022-1178
Preprint. Discussion started: 2 November 2022

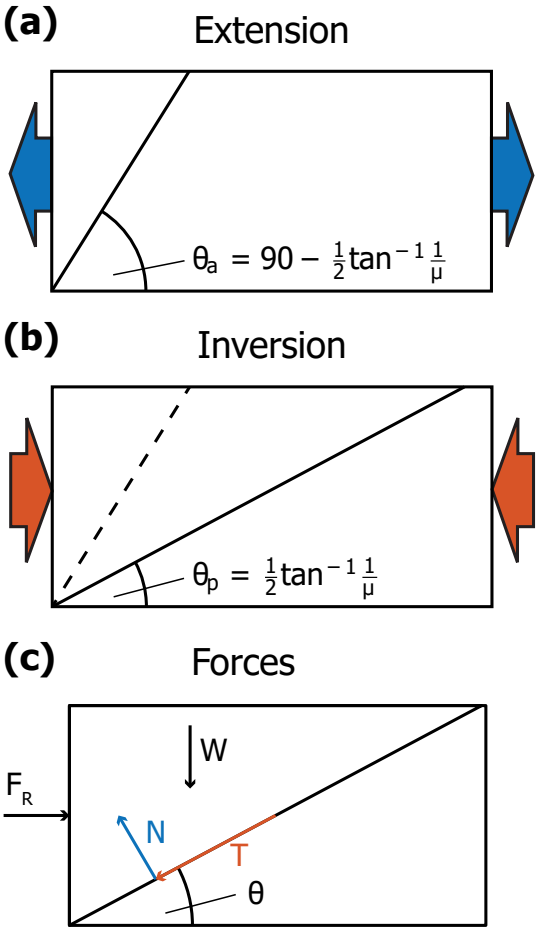

Figure 2. Definition of fault angles during a) extension and b) compression. In b) the preexisting fault is shown as a dashed line showing the difference in orientation. c) Force balance and definition of the force F_R required to move a block of weight W along a fault with an angle of θ (mod. after Mulugeta and Sokoutis, 2003)

https://doi.org/10.5194/egusphere-2022-1178
Preprint. Discussion started: 2 November 2022

$$F_R = \frac{\rho g h^2 \cot\theta}{2}\left[\frac{\mu + tan\,\theta}{1 - \mu\, tan\,\theta}\right] \tag{6}$$

A fault is considered severely misoriented when its angle is twice as large as the optimal fault angle. In this case the term $(1 - \mu\, tan\theta) \rightarrow 0$ which leads to extremely large values for F_R. In the lockup region $(1 - \mu\, tan\theta) < 0$ and therefore $F_R < 0$ which is unrealistic.

To account for healing, the friction for a reactivated fault is time dependent (i.e. increases with hold time) with the healing rate b as the power-law coefficient:

$$\mu_r(t) = \mu_0 t^b \tag{7}$$

This methodology neglects possible edge effects, such as shear stresses along the sidewall, because we assume a continuous granular layer that is cross-cut by several normal faults which are going to be inverted. Additionally, we do not incorporate changes in the stress field due to differences in elasticity of the material after healing and the formation of lower density shear bands that could lead to stress concentrations. Another important constraint of this simple model is, that it is not suitable for materials with higher cohesion because these tend to form surface cracks during extension leading to a change in fault angle with depth.

All calculations incorporate full uncertainty propagation through the Python module 'uncertainties' assuming normally distributed variables. For the frictional parameters μ, C and b the error given is 2 standard deviations calculated from the covariance of the fit and averaged per material (quartz sand, feldspar sand, glass beads, etc.). For density ρ the value is the arithmetic mean and error is 2 standard deviations of density for each material.

3 Results

3.1 Healing and Compaction Rates

We find that most materials exhibit healing rates in the range of $b <= 0.03$ (Figure 3), i.e., an increase in strength of less than 3% per tenfold increase in hold time increase of hold time (e.g. 10s vs 100s). Only two samples show healing rates that are not significantly different from zero, 'Freiburg' and 'Bern, CarloAG (100-300μm)' and are therefore considered to not show healing over experimental time scales. Most quartz sands show lower than average healing rates of roughly 1% per tenfold increase in hold time. Foam glass shows healing rates generally lower than those of quartz sands. Glass beads exhibit higher healing rates and show considerable spread between $b = 0.015$ and 0.025. Corundum sands are distributed over the full range of healing rates and feldspar sands overlap with glass beads. However, the number of samples for materials other than quartz sands and glass beads, is too small to generalize.

Compaction rates are more diverse and show a clearer separation between the materials (Figure 3b). Glass beads show the strongest compaction rates of $c = -0.055$ to -0.04 at the reference normal stress of $\sigma_N = 1kPa$. This means that sample

https://doi.org/10.5194/egusphere-2022-1178
Preprint. Discussion started: 2 November 2022

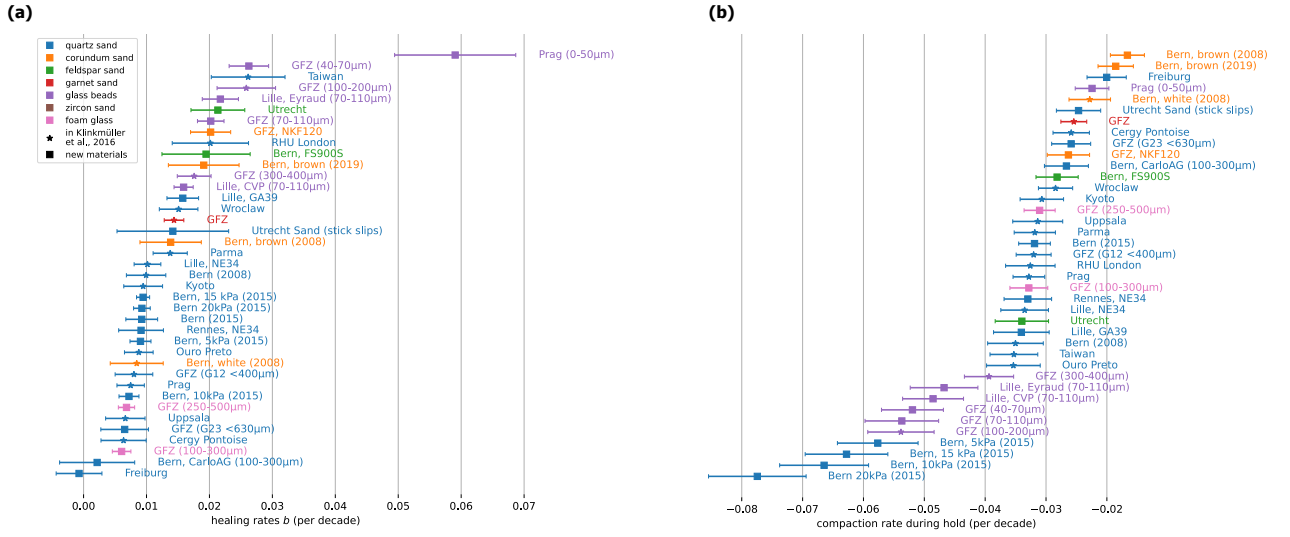

Figure 3. Stacked and sorted plot of (a) healing rates and (b) compaction rates for all tested materials. Similar materials often plot in the same range of healing or compaction rate. Notable exceptions are the healing rate for very fine glass beads (Prag, 0-50μm) and the compaction rates for higher normal stresses (Bern, 5kPa - 20kPa).

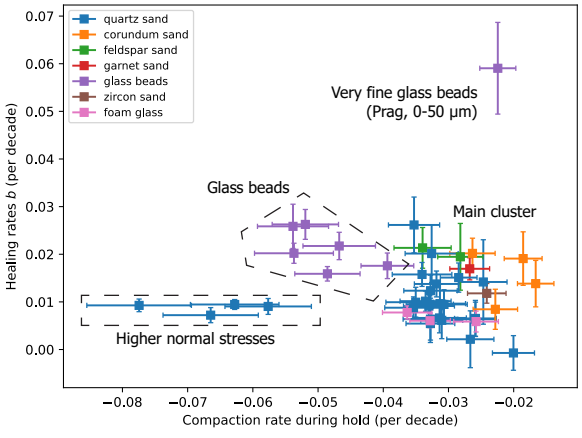

Figure 4. Comparison of healing rate and compaction rate. Materials that behave similarly are grouped in clusters.

thickness decreases by 4 to 5.5% per tenfold increase in hold time. The only exception are the very fine glass beads (Prag, 0-50μm) which show a very low compaction in comparison to the other glass bead samples. Quartz sands show small compaction rates between $c = -0.04$ and -0.02, with the majority of quartz sands having $c <= -0.03$. Feldspar sands and foam glass compaction rates are again comparable with quartz sands. In general, corundum sands exhibit the lowest compaction rates.

https://doi.org/10.5194/egusphere-2022-1178
Preprint. Discussion started: 2 November 2022

There is a strong influence of normal stresses on compaction which leads to much stronger compaction during hold. However, the healing rate is not significantly correlated with higher compaction and therefore the measurements with higher normal stresses form a distinct cluster when plotting compaction rate versus healing rate (Figure 4). Most samples do not show a clear distinction between sample material, compaction and healing rate. They all plot in a single cluster, with no significant correlation of compaction rate and healing rate. The glass beads are exceptional because they show high healing rates and high compaction rates, therefore forming a separate cluster. Using main and glass bead cluster, a weak negative correlation of healing rate and compaction rate is visible. An increase of healing with stronger compaction might be recognizable, albeit not statistically significant. The most notable exception are again the very fine glass beads (Prag, 0-50μm). These show a significantly stronger healing at small compaction rates.

3.2 Reactivation Properties

For the reactivation properties we summarized the samples into seven groups by taking the average and the standard deviation 2σ of all properties (friction coefficients μ, healing rate b and density ρ). As material height we choose $h = 0.05m$ that is comparable to a normal stress of $\sigma_N = 1000Pa$ for most materials and lies in the range of typical analogue model setups.

For the first phase of a typical basin inversion model the material is subjected to extensional stresses ($\sigma_1 \parallel S_v$, Equation 4) and fault angles are defined by the materials peak friction of $\mu_p = 0.50$ to 0.75 which results in $\theta_a = 58$ to $64°$ (dashed, coloured lines in Figure 5a-g). During compression the stress field changes ($\sigma_1 \parallel S_{hmax}$) and so does the angle of newly generated faults (Equation 5). The friction coefficient is the same because new faults mainly cross-cut undisturbed material and angles are in the range of $\theta_p = 26$ to $32°$ which leads to flatter faults in the model (solid, coloured lines in Figure 5a-g).

The lockup regions of all materials become increasingly larger, as reactivation friction μ_r increases over time. We find that for all materials, with the exception of glass beads, the angles of the preexisting faults fall within the lockup region. As a result, none of the faults that were created during extension should reactivate because they are severely misoriented. The optimal angle for reactivation, using the time-dependent μ_r is similar to the optimal angle of a new fault with μ_p which means that the difference in friction due to healing is not large enough to facilitate slip along inherited normal faults.

We find the same for the force required to move a wedge of material along the preexisting fault or the creation of a new fault (Figure 5h-n). For new faults the shear force per unit area ranges between $F_R = 50$ and $150\frac{N}{m}$ which means that for a triangular wedge of 5 cm height and 100 cm length in the direction of σ_2 between 50 and 150 N are required to initiate a new fault. While the height of the wedge has an influence on the absolute values of forces, the ratio between the forces $\frac{F_{new}}{F_{inherited}}$ is independent of height. For reactivated faults most materials show negative values and therefore reactivation is not possible.

The only exception are glass beads, which still are in the field of possible reactivation up to $t_h = 10^4\,s$ after shear. However, the stress required to reactivate these faults roughly is twice as high as for creating a new fault and reaches extremely high values already after $t_h = 10^3\,s$ (Figure 5l). A close inspection of the individual glass bead samples shows that glass beads with low grain sizes (e.g. GFZ, GB 70-110μm) are fully outside the lockup region. The stresses to reactivate these faults are only 1.5 to 2 times higher than the stress for new faults. The fault orientation is still more than 20 degrees away from the optimal

https://doi.org/10.5194/egusphere-2022-1178
Preprint. Discussion started: 2 November 2022

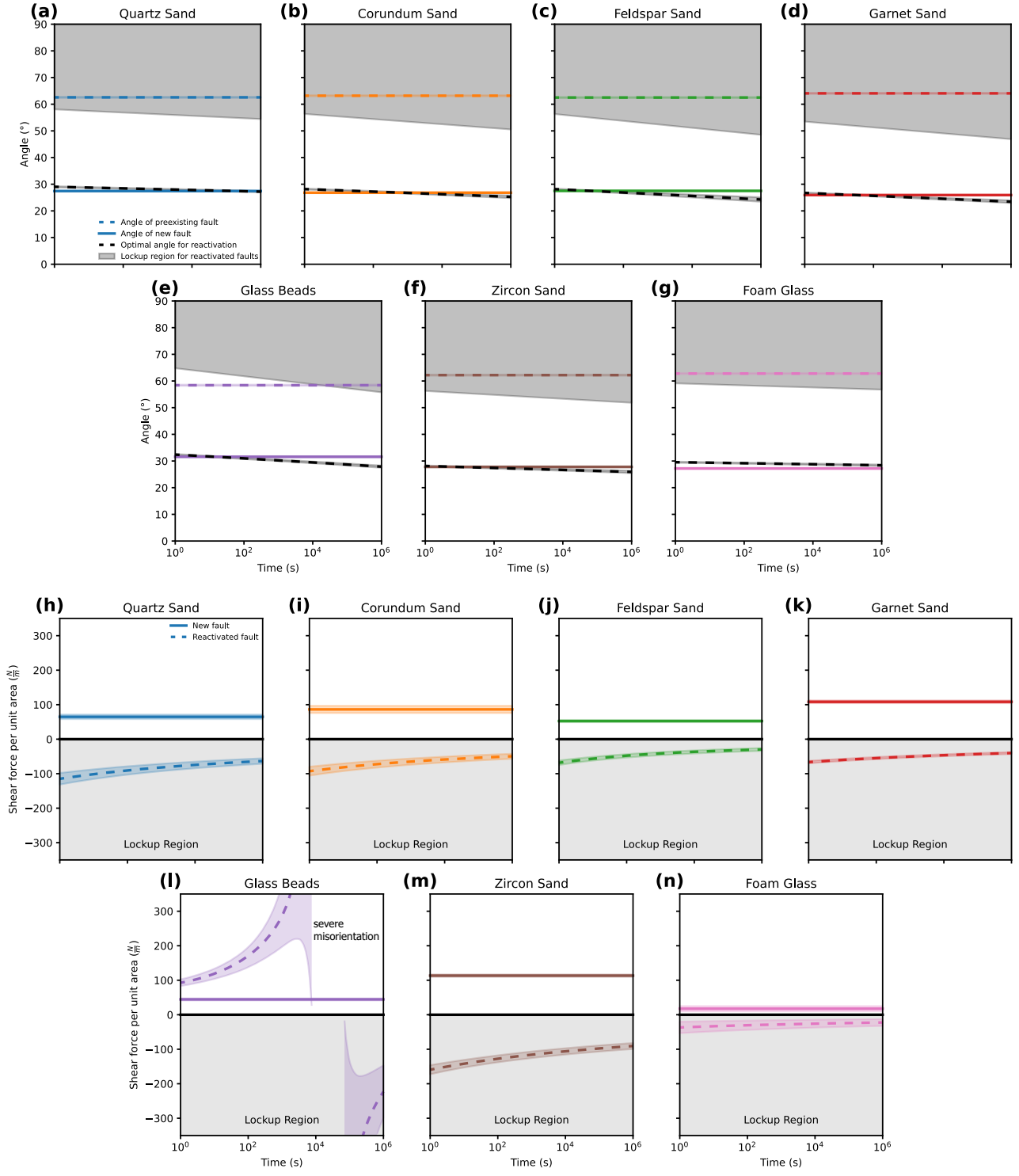

Figure 5. Optimal angles and shear forces for new and reactivated faults. a)-g) Optimal angles of faults for each material. h)-n) Shear forces required to move a wedge of material along a new and reactivated fault. Errorbars are derived from the uncertainties of the parameters and represent 2σ.

https://doi.org/10.5194/egusphere-2022-1178
Preprint. Discussion started: 2 November 2022

but under certain conditions a reactivation is possible for this sample. In general, reactivation is very unlikely despite the small difference between optimal and inherited angles.

3.3 Grain Characteristics

The materials are well sorted and very homogeneous because they are standardized industrial products for specific purposes. As a consequence, they contain no to few impurities, such as clay or pebbles, and are mostly monomineralic. Therefore, the properties presented here should apply to all batches from the same manufacturer. See Table A1 for a more detailed description of each sample and Figure A1 for a comparison of quality index with the frictional properties.

3.3.1 Quartz Sands

Quartz sands are the most frequently used analogue material and therefore represent the majority of samples. The color of most sands is yellowish to white with clear to translucent grains. Some sands are very homogeneous consisting of more than 99% quartz while others contain considerable (>5%) traces of feldspars, mica and other minerals. The sphericity is medium to high across all samples and differences are only minor. Roundness shows a larger spread with some rounded samples, such as the GFZ sands (Figure 6g), and some very angular sands, e.g. from Wroclaw. Roundness is mostly derived from the origin of the sands. Some sands are unprocessed eolian or fluvial sands which are (sub-)rounded, while others are processed and therefore show a high angularity due to crushing (Figure 6j). This division is also evident in the large spread of surface roughness. The sands that are rounded to subrounded generally have smoother surfaces. The angular sands often have shelly or jagged surfaces leading to high surface roughness. Some sands seemingly are mixtures of rounded and angular sands and therefore receive a lower score.

3.3.2 Glass Beads

Most glass beads show a very high sphericity, are perfectly rounded and have very smooth surfaces. Depending on the manufacturer, they are very well sorted and only have very few impurities (Figure 6e), e.g. glass beads from GFZ and Prag that are both supplied from the same manufacturer. Some samples either contain non-spherical grains (Figure 6f), fragments or a significant amount of beads that are sticking together or have small protrusions. This leads to a slightly lower score for sphericity and roundness. Usually, the glass beads are perfectly clear with a few whitish dots on the surface that probably stem from impacts of other beads during manufacture and transport.

3.3.3 Corundum Sands

The corundum sands, which are exlculsively processed (crushed) material, have medium sphericity with some elongated grains leading to a devaluation to a lower score in comparison to quartz sands. The color is yellowish, brown but transparent for the brown corundum sands and clear for white corundum. In general, they are very angular with sharp and pointy edges (Figure

https://doi.org/10.5194/egusphere-2022-1178
Preprint. Discussion started: 2 November 2022

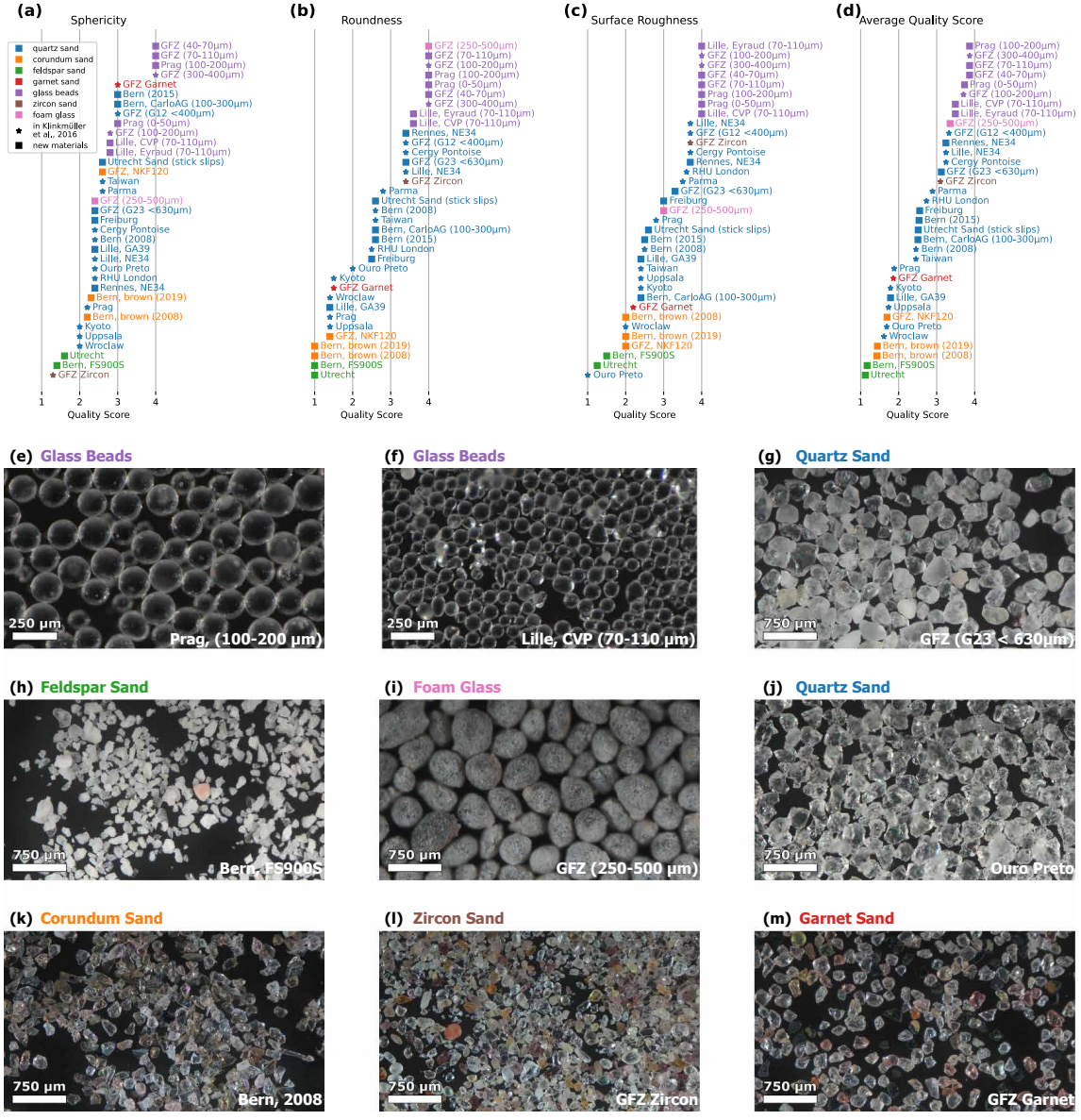

Figure 6. Quality scores and some exemplary materials that show specific characteristics. a)-d) Stacked and sorted quality score for the individual properties and weighted average according to Table 2. e) Glass beads with high sphericity, high roundness and low surface roughness. f) Glass beads with some low-sphericity grains. g) Typical quartz sand with medium sphericity, good roundness and low surface roughness (eolian sand). h) Feldspar sand with low sphericity, low roundness and high surface roughness. i) Foam glass with medium sphericity, good roundness and medium surface roughness. j) Sand with high surface roughness due to shelly and jagged surfaces (crushed sand). k) Corundum sand with some elongated grains leading to a higher sphericity score. l) Zircon sand with a many elongated and elliptical grains but with good roundness. m) Garnet sand with spherical, sub-angular grains and high surface roughness due to broken grains.

https://doi.org/10.5194/egusphere-2022-1178
Preprint. Discussion started: 2 November 2022

6k). This also leads to a high surface roughness, although the faces between the edges are generally flat and smooth. Some surfaces are shelly adding even more surface roughness. As a result, the average quality score is very low.

3.3.4 Feldspar Sands

The feldspar sands feature milky to translucent, white grains with low sphericity due to their elongated and triangular shape (Figure 6h). They are very angular and some seem to be aggregates of smaller grains. The surfaces are very rough with many sharp edges and surfaces, possibly due to cleavages. Most grains are internally fractured which contributes to the milky and translucent appearance. Therefore, the feldspar sands have the lowest average quality score.

3.3.5 Zircon Sands

The zircon sand, which is like corundum sands cruhed, is poorly sorted and contains a large variety of grain sizes and grain shapes (Figure 6l). Many grains are elongated and show the characteristic habit of zircon crystals, some seem to be fragments of these larger crystals. The color is reddish brown to off-white and the grains are translucent to clear. Depending on the grain size the grains are angular to rounded. Large grains tend to be well rounded and almost spherical while smaller ones are angular to sub-angular. The more or less intact crystals have sub-rounded crystal faces and edges. Due to the heterogeneous composition, the surface roughness also has a strong variation. The majority of grains has a smooth surface, however there are a few which show shelly or slightly rough surfaces.

3.3.6 Garnet Sands

On average the garnet sands show spherical with very few elongated grains (Figure 6m). They are mostly transparent with a reddish tint and about 10% of grains are dark and opaque. The transparent grains are angular to sub-angular and have a shelly surface. The darker grains are sub-rounded and have a slightly rough surface. Additionally, larger grains seem to be more rounded than smaller ones.

3.3.7 Foam Glass

Similar to the glass beads, the foam glasses are an industrially manufactured product and therefore are very homogeneous. No impurities could be found and the grain size distribution is very narrow and corresponds to the given specifications. They have a medium sphericity and have a ellipsoidal to random shape, similar to asteroids (Figure 6i). The color is gray and the grains are opaque. The grains are well rounded with no visible edges or faces. They have a very fine, sand paper like surface which leads to a slightly rough surface. Due to their surface roughness they rank just below the glass beads but still above the quartz sands.

https://doi.org/10.5194/egusphere-2022-1178
Preprint. Discussion started: 2 November 2022

4 Discussion

4.1 Reactivation of Faults in Basin Inversion Models

Our results show that for the tested materials the reactivation of inherited normal faults generated during extension as reverse faults should generally not be possible. This means that the difference between peak and reactivation friction of 5 to 15% is too small to create faults outside the lockup region (Sibson, 1980). Additionally, extensional faults in typical analogue models show higher angles than what is inferred from friction measurements with ring-shear testers (Panien et al., 2006). This is in accordance with the results of other studies that show only weak to no reactivation of preexisting structures in purely frictional sandbox models (Jara et al., 2018; Marques and Nogueira, 2008; Almilibia et al., 2005; Yagupsky et al., 2008; Molnar and Buiter, 2022). Due to their relatively low friction coefficient, glass beads are a certain exception. Reactivation is however still unlikely due to the high stresses required. As a consequence, many modelers use strong boundary conditions, such as heterogeneities or blocks, to force fault reactivation along specific normal faults (Bonini et al., 2000).

For setups that aim to reactivate extensional structures that are generated in situ, a possible solution could be to increase the amount of extension. On average the misorientation between lockup region and fault orientation is less than 10°. During extension the blocks rotate in a bookshelf like motion, thereby creating flatter fault angles. The stresses to reactivate faults close to the lockup regions are still quite high and therefore a rotation of ≈20° or more is required to lead to structures that can be reactivated. In analogue models the fault orientations usually show a larger spread than what is calculated in our theoretical model. The graben systems that form during extension usually contain several fault angles with flatter and steeper segments. Therefore, some faults could already be well within the reactivation field due to the heterogeneity in the analogue model, e.g. due to variation in bulk density.

Our model has limitations in quantifying the effect of cohesion on the reactivation of faults. The ring shear tests suggest that the reactivation cohesion is up to twice as high as peak cohesion for most materials which hinders fault reactivation even more. This effect is amplified for models with small thicknesses because for these the ratio of cohesive to gravitational stress is larger (Ritter et al., 2016a). To decrease the effect of cohesion the only option is to increase the normal stress by increasing the layer thickness. We note however, that cohesion is not directly measured here but is inferred from extrapolation. Because cohesion in granular materials used in analogue modelling is typically very small (few tens of Pa) or even zero, differences in cohesion might not be quantitatively sound.

4.2 Relation of Frictional Properties with Grain Characteristics

We compare the quality score of each material with all frictional parameters to recognize possible influences. To quantify correlations we calculate Pearson r and Spearman ρ correlation coefficients. We find that the healing rate b does show a weak positive correlation with sphericity ($r = 0.39$, $p = 0.05$; $\rho = 0.40$, $p = 0.04$) and is otherwise not correlated with any other quality measure. This means that with higher sphericity the materials tend to have higher healing rates. This is probably related to the compaction rate which shows a similar negative correlation with sphericity. Spherical grains compact more than aspherical beads which is evident from the higher compaction rates of glass beads (Figure 4). This is consistent with a tendency

https://doi.org/10.5194/egusphere-2022-1178
Preprint. Discussion started: 2 November 2022

of glass beads to compact more easily during cyclic axial loading tests reported by Klinkmüller et al. (2016). Higher sphericity is associated with lower void ratios before and after shearing (Härtl and Ooi, 2011) and therefore the individual grains are compacted more during a hold phase. In consequence, the stress required to mobilize these materials is higher because a larger amount of dilation is needed.

All three friction types (peak, reactivation and static) show a moderate negative correlation with all quality scores ($r \approx \rho \approx -0.6, p < 0.05$). As a result, there is a tendency to get lower frictional coefficients for materials that have high sphericity, higher roundness and smooth surfaces. The negative correlation of quality index with cohesion is very weak and has a much higher p-value leading to a higher uncertainty in the correlation. These results are in accordance with previous studies on granular characteristics Klinkmüller et al. (2016); Panien et al. (2006) and references in Table 2). We find a high correlation of peak friction with average quality score ($r = -0.70$, $\rho = -0.67$, $p = 0.01$) mostly influenced by the correlation of peak friction with roundness and surface quality.

The exceptionally high healing rate for very fine glass beads (Prag, 0-50μm) is probably the result of a strong increase in cohesion. In contrast to the other glass bead samples they do only show a small compaction rate, i.e., there is only a small reduction of density. Because of the wide particle size distribution and large amount of fine materials the void space is largely filled with finer glass powder. Additionally, very fine granular materials are susceptible to electrostatic effects that increase the attractive forces between particles.

4.3 Suitability for Modelling Natural Faults

Geodetic studies on postseismic surface motion demonstrate that faults quickly relock after a large earthquake (Bedford et al., 2016). We observe the same strong healing in the first few hold intervals caused by the power-law relation of strength and hold time (Equation 7) which is also observed for laboratory experiments on synthetic and natural fault rocks (Karner et al., 1997; Carpenter et al., 2016; Scuderi et al., 2014). Healing rates for dry synthetic and natural fault gouges range between 0.001 and 0.01 at room temperature (Ikari et al., 2016). Under wet conditions this healing rate can increase by one order of magnitude at temperatures $> 300°C$ (Niemeijer et al., 2008, and references therein). For gouges containing salt or salt-muscovite layers the rates are even higher.

Quartz sands and foam glass show healing rates that are generally low and closer to dry gouges while the glass beads, especially the very fine glass beads, have values that are closer to hydrothermal healing rates. However, the frictional strength is too low to use glass beads as well scaled analogues of self-healing faults in a model. A possibility might be the addition of a small percentage of fine material to sands thus achieving cohesion driven healing while retaining the overall higher bulk strength of sand. Such material mixes were not part of this study but can easily be tested with the methodology outlined here.

4.4 Implication of Healing Rates on Basin Inversion Models

Regardless of the mechanism creating the faults, most materials show a measurable amount of healing. The healing rates in the tested materials are low to moderate and lead to an increasingly larger lockup region over time. For materials that have high healing rates, e.g. glass beads, this increase is up to 1.5° per tenfold increase in hold time. This means that granular faults

https://doi.org/10.5194/egusphere-2022-1178
Preprint. Discussion started: 2 November 2022

that are about 12 hours old require a 7° lower angle to remain in the activity field. Depending on the type of setup this can change number of active faults, especially in graben systems consisting of several, similarly oriented faults. Healing can lead to a smaller amount of active faults when the time between fault creation and fault motion is increasing. In theory this should also apply to precut faults, because they alter the grain packaging in a similar way. This could even lead to the creation of new faults instead of localization at the predefined locations. However, with our methodology this is not verifiable and other mechanisms, such as the formation of shear fabrics in the granular material could play a role.

Due to the exponential nature of Equation 7 healing is very strong immediately after a fault comes to rest. Changing stress distribution in a running model commonly leads to constant, simultaneous activity on many faults. Therefore, only when a model is stopped, i.e, the model settles under the influence of gravity, healing can have a visible effect. The healing rates are small for most materials which means that only after several hours an effect on the reactivation angles is expected, even if the healing is strongest during the first few hours. In comparison with other processes, such as sieving technique or boundary conditions, fault healing only has a small, secondary influence on fault behaviour like the velocity dependence of friction during shear (Rosenau and Oncken, 2009). Consequently, if a model is continuously run without longer interruptions ($t_h < 1h$), the effect of healing is indistinguishable from other instantaneous mechanisms that influence an analogue fault's strength.

5 Conclusions

Healing rates and grain characteristics of a set of commonly used analogue materials from different laboratories were acquired through slide-hold-slide tests and by qualitative description. Furthermore, the reactivation potential of inherited normal faults in these materials was calculated using additional information from previous ring-shear tests. These experiments provide a better understanding of transient, time-dependent changes in analogue models and their potential impacts on the suitability of these materials for certain types of analogue models, such as basin inversion models. The experiments show that:

1. There is a measurable time dependency in brittle analogue models in the form of fault strengthening over the experimental timescale.

2. Healing rates are generally low but comparable to natural faults and gouges. The use of the tested analogue materials as analogues of healing faults might be possible. Glass beads show the highest amount of healing due to their spherical shape and smooth surface which leads to increased compaction during hold.

3. Reactivation of preexisting faults in the tested granular materials is very unlikely if the faults are not manually predefined. Fault orientations generated by extension are too steep and always lie in the lockup region. Only overextending with associated block rotation could lead to faults that are in the reactivation region. However, the generation of new faults is almost always energetically more favorable.

4. The frictional properties of most materials only show a weak correlation with grain characteristics. The strongest correlation was found for healing rates with sphericity and friction with average quality score. A general trend is that a low quality score roughly correlates with higher friction.

https://doi.org/10.5194/egusphere-2022-1178
Preprint. Discussion started: 2 November 2022

Code and data availability. All data is going to be available in the form of a data publication, together with Python scripts to generate all figures that use data. The python package 'granular-healing' for the analysis of slide-hold-slide tests is open-source and is part of the data publication as well as in a public git repository (https://git.gfz-potsdam.de/analab-code/granular-healing).

Video supplement. A video showing the experimental procedure of the ring-shear test is going to be available on the EPOS channel on youtube.com upon the publication of this manuscript.

https://doi.org/10.5194/egusphere-2022-1178
Preprint. Discussion started: 2 November 2022

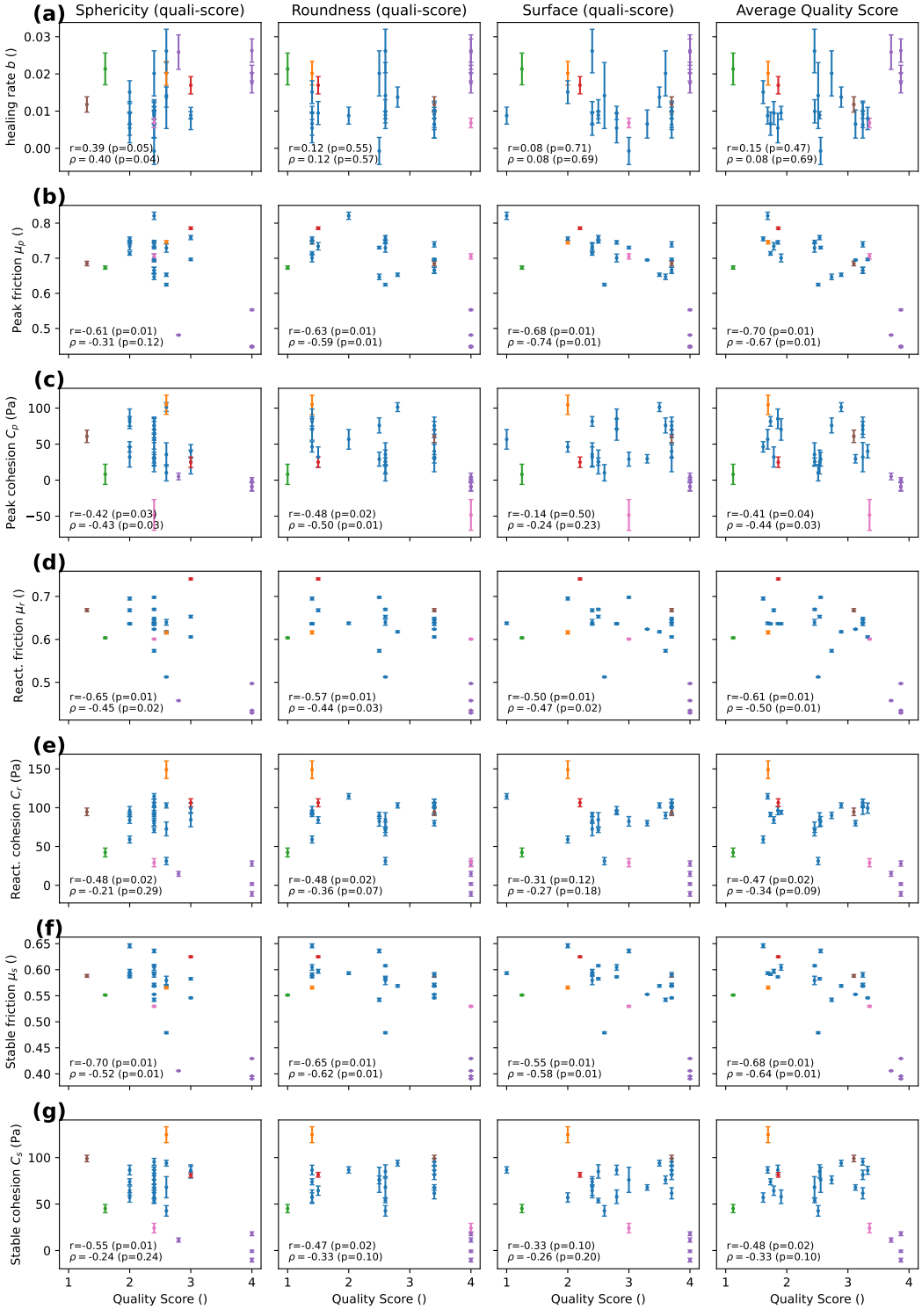

Figure A1. Correlation of all frictional properties with quality score.

https://doi.org/10.5194/egusphere-2022-1178
Preprint. Discussion started: 2 November 2022

Table A1. Description and quality score for each sample. Abbreviations: Qz - quartz, Crn - corundum, Fsp - feldspar, GB - glass beads, Grt - garnet, Zrn - zircon.

Sample		Sphericity		Roundness		Surface	
No.	Name	Description	Score	Description	Score	Description	Score
02	Qz sand, Bern Neusand	high	2	subrounded to subangular	2.4	slightly rough, shelly, some jagged	2.5
03	Qz sand, Utrecht 2018	high to medium	2.4	subrounded to subangular	2.4	sightly rough, shelly	2.4
05	Qz sand, Rennes NE34 2021	medium to high	2.6	subrounded to rounded	1.6	smooth, few shelly, few slightly rough	1.3
06	Qz sand, Parma	high to medium	2.4	subrounded, few subangular	2.2	smooth, shelly	1.5
07	Qz sand, Kyoto	medium	3	angular to subangular, few subrounded	3.5	shelly, slightly rough	2.6
08	Qz sand, Bern 2008	medium to high	2.6	subrounded to subangular	2.4	slightly rough, shelly, some jagged	2.5
09	Crn sand, GFZ NKF120	high to medium	2.4	angular to subangular	3.6	shelly	3
10	Qz sand, Uppsala	medium	3	angular to subangular	3.6	shelly, slightly rough	2.6
11	Qz sand, Cergy Pontoise	medium to high	2.6	subrounded to rounded	1.6	smooth, few shelly, few slightly rough	1.3
12	Crn sand, Bern 2019	medium to high, few elongated grains	2.7	angular	4	shelly	3
13	Fsp sand, Utrecht	medium to low	3.4	angular	4	jagged, rough	3.75
14	Qz sand, RHU-London	medium to high	2.6	subangular, some angular, some rounded	2.5	smooth, some shelly	1.4
15	Qz sand, GFZ G12 $<400\mu m$	high	2	subrounded to rounded	1.6	smooth, few shelly, few slightly rough	1.3
16	Qz sand, GFZ G23 $<630\mu m$	medium to high	2.6	subrounded to rounded	1.6	slightly rough, smooth, few shelly	1.7
17	Qz sand, Prag ST55	medium	3	angular to subangular	3.6	slightly rough, few shelly	2.2
18	Grt sand, GFZ 2008	high	2	angular to sub angular, few rounded	3.5	shelly, few slightly rough to smooth	2.8
19	GB 70-110μm, GFZ	perfect	1	rounded	1	smooth	1
20	GB 300-400μm, GFZ	perfect	1	rounded	1	smooth	1
21	GB 40-70μm, GFZ	perfect	1	rounded	1	smooth	1
22	GB 100-200μm, GFZ	high, some medium	2.2	rounded	1	smooth	1
23	Zrn sand, GFZ 2009	low to medium, several elongated grains	3.7	subrounded to rounded	1.6	smooth, few shelly, few slightly rough	1.3
25	GB 0-50 μm, Prag poured	high	2	rounded	1	smooth	1
26	GB 100-200μm, Prag	perfect	1	rounded	1	smooth	1
28	Qz sand, Bern CarloAG 100-300μm	high	2	subrounded to subangular	2.4	shelly, slightly rough	2.6
35	Fsp sand, Bern FS900S	low to medium	3.6	angular	4	rough, jagged	3.5
36	Qz sand, Lille G39	medium to high	2.6	angular to subangular	3.6	shelly, slightly rough	2.6
37	Qz sand, Lille NE34	medium to high	2.6	subrounded to rounded	1.6	smooth, few shelly, few slightly rough	1.3
38	GB 70-110μm, Lille CVP	high, some medium	2.2	rounded to subrounded	1.4	smooth	1
39	GB 70-110μm, Lille Eyraud	high, some medium	2.2	rounded to subrounded	1.4	smooth	1
40	Qz sand, Prague	medium to high	2.6	angular to subangular	3.6	slightly rough, few shelly	2.2
41	Qz sand, Wroclaw	medium	3	angular to subangular	3.6	shelly	3
42	Qz sand, Taiwan	high to medium	2.4	subrounded to subangular	2.4	shelly, slightly rough	2.6
43	Qz sand, OuroPreto	medium to high	2.6	subangular	3	jagged	4
45	Crn sand, Bern	medium to high, some elongated grains	2.8	angular	4	shelly	3
46	Qz sand, Freiburg	medium to high	2.6	subangular to round	2.5	some smooth, some jagged	2
47	Foam glass 250-500μm, GFZ	medium to high	2.6	rounded	1	slightly rough	2

https://doi.org/10.5194/egusphere-2022-1178
Preprint. Discussion started: 2 November 2022

Author contributions. Conceptualization of this project was done by MRu and MRo. Measurements were done by MRu and MRo. Data analysis and programming was done by MRu. The manuscript was written by MRu with the help of MRo and OO. All authors read and approved the final manuscript.

Competing interests. The authors declare that no competing interests are present.

Acknowledgements. We thank all participants from the laboratories who sent their samples to be tested for this study. The authors thank the technical staff at the Helmholtz Laboratory for Tectonic Modelling for running some of the long-term tests (F. Neumann) and for setting up the monitoring devices (T. Ziegenhagen). We kindly thank J. Mingram (GFZ Potsdam) and L. Stutenbecker (TU Darmstadt) for providing support and access to the microscopes at their institutes. This research has been partially funded by Deutsche Forschungsgemeinschaft (DFG) through grant number 235221301 - CRC 1114 "Scaling Cascades in Complex Systems", Project B01 "Fault networks and scaling properties of deformation accumulation".

https://doi.org/10.5194/egusphere-2022-1178
Preprint. Discussion started: 2 November 2022

References

Almilibia, A., Mc Clay, K., i Montserrat, F. S., Muñoz, J., and Roca, E.: Analogue modelling of inverted oblique rift systems, Geologica Acta, pp. 251–251, 2005.

ASTM, D.: Test Method for Bulk Solids Using Schulze Ring Shear Tester, https://doi.org/10.1520/d6773-16, 2016.

Bedford, J., Moreno, M., Li, S., Oncken, O., Baez, J. C., Bevis, M., Heidbach, O., and Lange, D.: Separating rapid relocking, afterslip, and viscoelastic relaxation: An application of the postseismic straightening method to the Maule 2010 cGPS, Journal of Geophysical Research: Solid Earth, 121, 7618–7638, https://doi.org/10.1002/2016jb013093, 2016.

Beeler, N., Tullis, T., and Weeks, J.: The roles of time and displacement in the evolution effect in rock friction, Geophysical Research Letters, 21, 1987–1990, https://doi.org/10.1029/94gl01599, 1994.

Bhattacharya, P., Rubin, A. M., and Beeler, N. M.: Does fault strengthening in laboratory rock friction experiments really depend primarily upon time and not slip?, Journal of Geophysical Research: Solid Earth, 122, 6389–6430, 2017.

Bonini, M., Sokoutis, D., Mulugeta, G., and Katrivanos, E.: Modelling hanging wall accommodation above rigid thrust ramps, Journal of Structural geology, 22, 1165–1179, https://doi.org/10.1016/s0191-8141(00)00033-x, 2000.

Bonini, M., Sani, F., and Antonielli, B.: Basin inversion and contractional reactivation of inherited normal faults: A review based on previous and new experimental models, Tectonophysics, 522-523, 55–88, https://doi.org/10.1016/j.tecto.2011.11.014, 2012.

Buchanan, J. G., Buchanan, P. G., and Ziegler, P.: Basin inversion, vol. 88, Geological Society London, https://doi.org/10.1144/GSL.SP.1995.088.01.30, 1995.

Carpenter, B. M., Ikari, M. J., and Marone, C.: Laboratory observations of time-dependent frictional strengthening and stress relaxation in natural and synthetic fault gouges, Journal of Geophysical Research: Solid Earth, 121, 1183–1201, 2016.

Cates, M., Wittmer, J., Bouchaud, J.-P., and Claudin, P.: Jamming, force chains, and fragile matter, Physical review letters, 81, 1841, https://doi.org/10.1103/physrevlett.81.1841, 1998.

Chen, C., Gu, J., Peng, Z., Dai, X., Liu, Q., and Zhu, G.-Q.: Discrete element modeling of particles sphericity effect on sand direct shear performance, Scientific Reports, 12, https://doi.org/10.1038/s41598-022-09543-9, 2022.

Collettini, C. and Sibson, R. H.: Normal faults, normal friction?, Geology, 29, 927, https://doi.org/10.1130/0091-7613(2001)029<0927:nfnf>2.0.co;2, 2001.

da Cruz, F., Emam, S., Prochnow, M., Roux, J.-N., and Chevoir, F.: Rheophysics of dense granular materials: Discrete simulation of plane shear flows, Physical Review E, 72, 021 309, https://doi.org/10.1103/physreve.72.021309, 2005.

Daniels, K. E. and Hayman, N. W.: Force chains in seismogenic faults visualized with photoelastic granular shear experiments, J. Geophys. Res., 113, https://doi.org/10.1029/2008jb005781, 2008.

Dieterich: Time-Dependent Friction and the Mechanics of Stick-Slip, Pageoph, 116, 1978.

Dieterich, J.: Applications of rate-and state-dependent friction to models of fault slip and earthquake occurrence, Treatise on Geophysics, 4, 107–129, https://doi.org/10.1016/b978-044452748-6.00065-1, 2007.

Hubbert, M. K.: Theory of scale models as applied to the study of geologic structures, Geological Society of America Bulletin, 48, 1459–1520, 1937.

Härtl, J. and Ooi, J. Y.: Numerical investigation of particle shape and particle friction on limiting bulk friction in direct shear tests and comparison with experiments, Powder Technology, 212, 231–239, https://doi.org/https://doi.org/10.1016/j.powtec.2011.05.022, 2011.

https://doi.org/10.5194/egusphere-2022-1178
Preprint. Discussion started: 2 November 2022

Ikari, M. J., Carpenter, B. M., and Marone, C.: A microphysical interpretation of rate- and state-dependent friction for fault gouge, Geochemistry, Geophysics, Geosystems, 17, 1660–1677, https://doi.org/10.1002/2016gc006286, 2016.

Jara, P., Likerman, J., Charrier, R., Herrera, S., Pinto, L., Villarroel, M., and Winocur, D.: Closure type effects on the structural pattern of an inverted extensional basin of variable width: Results from analogue models, Journal of South American Earth Sciences, 87, 157–173, https://doi.org/10.1016/j.jsames.2017.10.018, 2018.

Karner, S. L., Marone, C., and Evans, B.: Laboratory study of fault healing and lithification in simulated fault gouge under hydrothermal conditions, Tectonophysics, 277, 41–55, https://doi.org/10.1016/s0040-1951(97)00077-2, 1997.

Kato, N. and Tullis, T. E.: A composite rate-and state-dependent law for rock friction, Geophysical research letters, 28, 1103–1106, 2001.

Klinkmüller, M., Schreurs, G., Rosenau, M., and Kemnitz, H.: Properties of granular analogue model materials: A community wide survey, Tectonophysics, 684, 23–38, https://doi.org/10.1016/j.tecto.2016.01.017, 2016.

Lohrmann, J., Kukowski, N., Adam, J., and Oncken, O.: The impact of analogue material properties on the geometry, kinematics, and dynamics of convergent sand wedges, Journal of Structural Geology, 25, 1691–1711, https://doi.org/10.1016/s0191-8141(03)00005-1, 2003.

Mair, K., Frye, K. M., and Marone, C.: Influence of grain characteristics on the friction of granular shear zones, Journal of Geophysical Research: Solid Earth, 107, https://doi.org/10.1029/2001jb000516, 2002.

Marone, C.: Laboratory-derived friction laws and their application to seismic faulting, Annual Review of Earth and Planetary Sciences, 26, 643–696, https://doi.org/10.1146/annurev.earth.26.1.643, 1998.

Marques, F. and Nogueira, C.: Normal fault inversion by orthogonal compression: Sandbox experiments with weak faults, Journal of Structural Geology, 30, 761–766, https://doi.org/10.1016/j.jsg.2008.02.015, 2008.

Molnar, N. and Buiter, S.: Analogue modelling of the inversion of multiple extensional basins in foreland fold-and-thrust belts, EGUsphere, 2022, 1–35, https://doi.org/10.5194/egusphere-2022-1014, 2022.

Montanari, D., Agostini, A., Bonini, M., Corti, G., and Ventisette, C.: The Use of Empirical Methods for Testing Granular Materials in Analogue Modelling, Materials, 10, 635, https://doi.org/10.3390/ma10060635, 2017.

Mulugeta, G. and Sokoutis, D.: Hanging wall accommodation styles in ramp-flat thrust models, Geological Society, London, Special Publications, 212, 197–207, https://doi.org/10.1144/gsl.sp.2003.212.01.13, 2003.

Nagata, K., Nakatani, M., and Yoshida, S.: A revised rate-and state-dependent friction law obtained by constraining constitutive and evolution laws separately with laboratory data, Journal of Geophysical Research: Solid Earth, 117, 2012.

Niemeijer, A., Marone, C., and Elsworth, D.: Healing of simulated fault gouges aided by pressure solution: Results from rock analogue experiments, Journal of Geophysical Research, 113, https://doi.org/10.1029/2007jb005376, 2008.

Panien, M., Schreurs, G., and Pfiffner, A.: Mechanical behaviour of granular materials used in analogue modelling: insights from grain characterisation, ring-shear tests and analogue experiments, Journal of Structural Geology, 28, 1710–1724, 2006.

Pohlenz, A., Rudolf, M., Kemnitz, H., and Rosenau, M.: Ring shear test data of glass beads 40-70 μm used for analogue experiments in the Helmholtz Laboratory for Tectonic Modelling (HelTec) at the GFZ German Research Centre for Geosciences in Potsdam, https://doi.org/10.5880/GFZ.4.1.2020.006, 2020a.

Pohlenz, A., Rudolf, M., Kemnitz, H., and Rosenau, M.: Ring shear test data of glass beads 70-110 μm used for analogue experiments in the Helmholtz Laboratory for Tectonic Modelling (HelTec) at the GFZ German Research Centre for Geosciences in Potsdam, https://doi.org/10.5880/GFZ.4.1.2020.007, 2020b.

https://doi.org/10.5194/egusphere-2022-1178
Preprint. Discussion started: 2 November 2022

Pohlenz, A., Rudolf, M., Kemnitz, H., and Rosenau, M.: Ring shear test data of glass beads 300-400 μm used for analogue experiments in the Helmholtz Laboratory for Tectonic Modelling (HelTec) at the GFZ German Research Centre for Geosciences in Potsdam, https://doi.org/10.5880/GFZ.4.1.2020.008, 2020c.

Poppe, S., Holohan, E. P., Rudolf, M., Rosenau, M., Galland, O., Delcamp, A., and Kervyn, M.: Mechanical properties of quartz sand and gypsum powder (plaster) mixtures: Implications for laboratory model analogues for the Earth's upper crust, Tectonophysics, 814, 228 976, https://doi.org/10.1016/j.tecto.2021.228976, 2021a.

Poppe, S., Holohan, E. P., Rudolf, M., Rosenau, M., Galland, O., Delcamp, A., Van Gompel, G., Buls, N., Soens, B., Pohlenz, A., Mourgues, R., and Kervyn, M.: Mechanical test data of quartz sand, garnet sand, gypsum powder (plaster), kaolin and sand-plaster mixtures used as granular analogue materials in geoscience laboratory experiments, https://doi.org/10.5880/FIDGEO.2021.005, 2021b.

Ritter, M. C., Leever, K., Rosenau, M., and Oncken, O.: Scaling the Sand Box - Mechanical (Dis-) Similarities of Granular Materials and Brittle Rock, J. Geophys. Res. Solid Earth, https://doi.org/10.1002/2016jb012915, 2016a.

Ritter, M. C., Leever, K., Rosenau, M., and Oncken, O.: Supplement to: Scaling the Sand Box - Mechanical (Dis-) Similarities of Granular Materials and Brittle Rock, GFZ Data Services, https://doi.org/10.5880/GFZ.4.1.2016.005, 2016b.

Ritter, M. C., Rosenau, M., and Oncken, O.: Growing Faults in the Lab: Insights Into the Scale Dependence of the Fault Zone Evolution Process, Tectonics, 37, 140–153, https://doi.org/10.1002/2017tc004787, 2018.

Román-Berdiel, T., Casas, A. M., Pueyo, E. L., Peiro Chamarro, A., Soto, R., Pohlenz, A., Warsitzka, M., and Rosenau, M.: Ring shear test data of quartz sand and colored quartz sand used for analogue modelling in the Laboratorio de modelización analógica, Universidad de Zaragoza, Spain (EPOS TNA call 2017)., https://doi.org/10.5880/FIDGEO.2019.025, 2019.

Rosenau, M. and Oncken, O.: Fore-arc deformation controls frequency-size distribution of megathrust earthquakes in subduction zones, Journal of Geophysical Research: Solid Earth (1978–2012), 114, https://doi.org/10.1029/2009jb006359, 2009.

Rosenau, M., Pohlenz, A., Kemnitz, H., and Warsitzka, M.: Ring-shear test data of quartz sand G12 used for analogue experiments in the Helmholtz Laboratory for Tectonic Modelling (HelTec) at the GFZ German Research Centre for Geosciences in Potsdam, https://doi.org/10.5880/GFZ.4.1.2019.003, 2018a.

Rosenau, M., Pohlenz, A., Kemnitz, H., and Warsitzka, M.: Ring-shear test data of quartz sand G23 used for analogue experiments in the Helmholtz Laboratory for Tectonic Modelling (HelTec) at the GFZ German Research Centre for Geosciences in Potsdam, https://doi.org/10.5880/GFZ.4.1.2019.004, 2018b.

Rudolf, M.: RST-Stick-Slipy, GFZ Data Services, https://doi.org/10.5880/GFZ.4.1.2021.007, 2021.

Rudolf, M. and Warsitzka, M.: RST Evaluation - Scripts for analysing shear experiments from the Schulze RST.pc01 ring shear tester, https://doi.org/10.5880/GFZ.4.1.2021.001, 2021.

Rudolf, M., Boutelier, D., Rosenau, M., Schreurs, G., and Oncken, O.: Rheological benchmark of silicone oils used for analog modeling of short-and long-term lithospheric deformation, Tectonophysics, https://doi.org/10.1016/j.tecto.2015.11.028, 2016.

Rudolf, M., Rosenau, M., and Oncken, O.: The spectrum of slip behaviours of a granular fault gouge analogue governed by rate and state friction, Geochemistry, Geophysics, Geosystems, 22, https://doi.org/10.1029/2021GC009825, 2021.

Ruina, A.: Slip instability and state variable friction laws, Journal of Geophysical Research: Solid Earth, 88, 10 359–10 370, https://doi.org/10.1029/jb088ib12p10359, 1983.

Schmid, T., Schreurs, G., Warsitzka, M., and Rosenau, M.: Effect of sieving height on density and friction of brittle analogue material: Ring-shear test data of corundum sand used for analogue experiments in the Tectonic Modelling Lab of the University of Bern (CH), https://doi.org/10.5880/FIDGEO.2020.005, 2020.

https://doi.org/10.5194/egusphere-2022-1178
Preprint. Discussion started: 2 November 2022

Scholz, C. H.: The mechanics of earthquakes and faulting, Cambridge university press, 2002.

Schulze, D.: Development and application of a novel ring shear tester, Aufbereitungs Technik, 35, 524–535, 1994.

Schulze, D.: Powders and bulk solids, Springer, 2008.

Scuderi, M. M., Carpenter, B. M., and Marone, C.: Physicochemical processes of frictional healing: Effects of water on stick-slip stress drop and friction of granular fault gouge, Journal of Geophysical Research: Solid Earth, 119, 4090–4105, https://doi.org/10.1002/2013jb010641, 2014.

Sibson, R. H.: Power dissipation and stress levels on faults in the upper crust, Journal of Geophysical Research: Solid Earth, 85, 6239–6247, https://doi.org/https://doi.org/10.1029/JB085iB11p06239, 1980.

Suh, H. S., Kim, K. Y., Lee, J., and Yun, T. S.: Quantification of bulk form and angularity of particle with correlation of shear strength and packing density in sands, Engineering Geology, 220, 256–265, https://doi.org/10.1016/j.enggeo.2017.02.015, 2017.

Tapia, F., Pouliquen, O., and Guazzelli, É.: Influence of surface roughness on the rheology of immersed and dry frictional spheres, Physical Review Fluids, 4, 104 302, https://doi.org/10.1103/physrevfluids.4.104302, 2019.

Turner, J. P. and Williams, G. A.: Sedimentary basin inversion and intra-plate shortening, Earth-Science Reviews, 65, 277–304, https://doi.org/https://doi.org/10.1016/j.earscirev.2003.10.002, 2004.

Warsitzka, M., Ge, Z., Schönebeck, J.-M., Pohlenz, A., and Kukowski, N.: Ring-shear test data of foam glass beads used for analogue experiments in the Helmholtz Laboratory for Tectonic Modelling (HelTec) at the GFZ German Research Centre for Geosciences in Potsdam and the Institute of Geosciences, Friedrich Schiller University Jena, https://doi.org/10.5880/GFZ.4.1.2019.002, 2019a.

Warsitzka, M., Závada, P., Pohlenz, A., and Rosenau, M.: Ring-shear test data of quartz sand used for analogue experiments in the laboratory of the Institute of Geophysics of the Czech Academy of Science, Prague, https://doi.org/10.5880/GFZ.4.1.2019.008, 2019b.

Willingshofer, E., Sokoutis, D., Beekman, F., Schönebeck, J.-M., Warsitzka, M., and Rosenau, M.: Ring shear test data of feldspar sand and quartz sand used in the Tectonic Laboratory (TecLab) at Utrecht University for experimental Earth Science applications, https://doi.org/10.5880/FIDGEO.2018.072, 2018.

Yagupsky, D. L., Cristallini, E. O., Fantín, J., Valcarce, G. Z., Bottesi, G., and Varadé, R.: Oblique half-graben inversion of the Mesozoic Neuquén Rift in the Malargüe Fold and Thrust Belt, Mendoza, Argentina: New insights from analogue models, Journal of Structural Geology, 30, 839–853, https://doi.org/10.1016/j.jsg.2008.03.007, 2008.

Yasuhara, H., Marone, C., and Elsworth, D.: Fault zone restrengthening and frictional healing: The role of pressure solution, Journal of Geophysical Research: Solid Earth, 110, https://doi.org/https://doi.org/10.1029/2004JB003327, 2005.

Zwaan, F., Schreurs, G., Gentzmann, R., Warsitzka, M., and Rosenau, M.: Ring-shear test data of quartz sand from the Tectonic Modelling Lab of the University of Bern (CH), https://doi.org/10.5880/FIDGEO.2018.028, 2018.